Void fraction measurement of gas-liquid two-phase flow with a 12-electrode contactless resistivity array sensor under different excitation patterns

Zhen Xu1, Yandan Jiang1, Baoliang Wang1, Haifeng Ji1, Zhiyao Huang1* and Manuchehr Soleimani2*

[1] State Key Laboratory of Industrial Control Technology, College of Control Science and Engineering
Zhejiang University, Hangzhou 310027, China
[2] Engineering Tomography Laboratory (ETL), Department of Electronic and Electrical Engineering,
University of Bath, Bath BA2 7AY, United Kingdom

E-mail: zy_huang@zju.edu.cn and M.Soleimani@bath.ac.uk

Abstract

This work focuses on the void fraction measurement of gas-liquid two-phase flow by a 12-electrode contactless resistivity array sensor. A 12-electrode contactless resistivity array sensor, which can realize different excitation patterns, is developed. Five different excitation patterns (1-electrode excitation pattern, 2-electrode excitation pattern, 3-electrode excitation pattern, 4-electrode excitation pattern and 5-electrode excitation pattern) and three two-phase distributions (bubble flow, stratified flow and annular flow) are investigated. Two data processing approaches, the data average method and the principal component regression (PCR) method, are used to establish the void fraction measurement models and hence to implement the void fraction measurement. With the 12-electrode contactless resistivity array sensor, void fraction measurement experiments are carried out. Experimental results show that the void fraction measurement performances are different under different excitation patterns. Among the studied five different excitation patterns, the 5-electrode excitation pattern has the best void fraction measurement performance and the absolute values of void fraction measurement errors of the three two-phase distributions are all less than 5.0% (using data average method) and 3.0% (using PCR method). Research results indicate that the 5-electrode excitation pattern + PCR combination is a new effective way to implement void fraction measurement of gas-liquid two-phase flow with the 12-electrode contactless resistivity array sensor.

Keywords: void fraction, gas-liquid two-phase flow, array sensor, contactless resistivity measurement, modelling method

1. Introduction

Gas-liquid two-phase flow has a wide range of applications in industry such as chemical, petroleum, energy, power engineering, etc. Void fraction is a fundamental parameter of the gas-liquid two-phase flow, which is very important for safety control, environment protection, energy conservation and quality assurance in industry [1-19].

The conductivity of conductive gas-liquid two-phase flow contains significant information about phase distribution and void fraction of the flow. The method on the basis of contact conductivity measurement is a classic method for void fraction measurement of conductive gas-liquid two-phase flow and has been studied for decades [1-19]. To overcome the influence of different flow patterns (phase distributions) on void fraction measurement, using multi-electrode conductivity array sensor is an important approach [3-19].

Merilo et al. set up a rotating electric field inside a pipe by applying a three-phase signal to the three pairs of opposing electrodes and established the relationship between the void fraction and the relative conductivity [3, 5]. Tournaire used a two-electrode void meter with single-phase a.c. supply, a four-electrode void meter with single-phase a.c. supply and a six-electrode void meter with six-phase a.c. supply to measure the void fraction of two-phase flow with resistance data. It was found that the void meter with six-phase a.c. supply had better measurement results [3, 6]. Andreussi et al. used a conductance probe with three ring electrodes to measure the void fraction in liquid slugs for air-water flow in horizontal and near-horizontal pipes with a semi-empirical correlation [3, 7]. Saiz et al. used the resistance data obtained from two types of sensors (2-electrode "fixed" electrical field and 6-electrode "rotating" electrical field) to measure the propagation of small void fraction disturbances along an upward vertical test section [3, 8]. Chase et al. detected the averaging volume of multiphase flow by 2-electrode electroconductivity probes and designed the probes sizing the characteristic length between the electrodes [3, 9]. Fossa et al. used two pairs of flush electrodes, which were ring-shaped and plate electrodes, to measure the void fraction of gas-liquid mixtures in pipes by conductance data [10]. Devia et al. investigated the impedance probes with electrodes of different shapes to improve the probe response and implemented the void fraction measurement of different flow patterns with the measured conductance data [11]. Dong et al. measured the void fraction of gas-liquid two-phase flow by data from a sixteen-electrode electrical resistance sensor [12]. Cho et al. used a pair of flush-mounted electrodes to measure the volume fraction of the disperse phase in a stratified near-wall bubbly flow with the bulk conductivity (and the known electrical conductivity of the continuous and disperse phases) [13]. Rocha et al. developed two 8-electrode impedance probes and established a rotating electric field sweeping across the test section to measure the void fraction of air-water two-phase flow with the calibration curve between the void fraction and the dimensionless conductivity [14]. Borges et al. combined a three-hole pressure probe with back-flushing with a conductivity probe to measure void fraction in air-water flows [15]. Zhao et al. developed a wireless 4-electrode electrical resistance detector (WERD) to measure the real-time particle volume fraction in centrifugal fields [16]. Dang et al. used a multi single-sensor conductivity probe to measure the local time-averaged void fraction of two-phase flow. The advantage of multi single-sensor probe was to reduce the experiment time [17]. Dang et al. estimated the void fraction of two-phase flow with an eigenvalue analysis of EIT raw data with a 16-electrode EIT sensor and the conductivity signal of two-phase flow was adopted [18]. Forte et al. used an 18-electrode electrical resistance tomography (ERT) linear probe to measure gas holdup in a two-phase (gas–liquid) flow [19]. All the above research works provide useful experience and reference for the void fraction measurement of two-phase flow. However, most of these research works are based on the contact conductivity detection which will lead to electrochemical erosion and polarization effect of the electrodes. Besides, the current void fraction measurement performance still cannot meet the increasing requirements of practical applications of gas–liquid two-phase flow. More research should be done.

Capacitively coupled contactless conductivity detection (C^4D) technique has provided an effective approach for contactless conductivity measurement [20-21]. Figure 1 shows the measurement principle of the C^4D technique. Figure 1(1) shows the construction of a radial C^4D sensor, which includes the insulating pipe, the excitation electrode, the detection electrode and the current pick-up unit. Figure 1(2) shows the simplified equivalent circuit of the measurement electrode pair, i.e., an AC path constituted by two coupling capacitors (formed by the two electrodes, the insulating pipe and the measured fluid) and a resistor (formed by the conductive fluid). When an AC voltage excitation signal u_i is generated on the excitation electrode, an AC current signal i_o can be obtained on the detection electrode and then processed by the current pick-up unit.

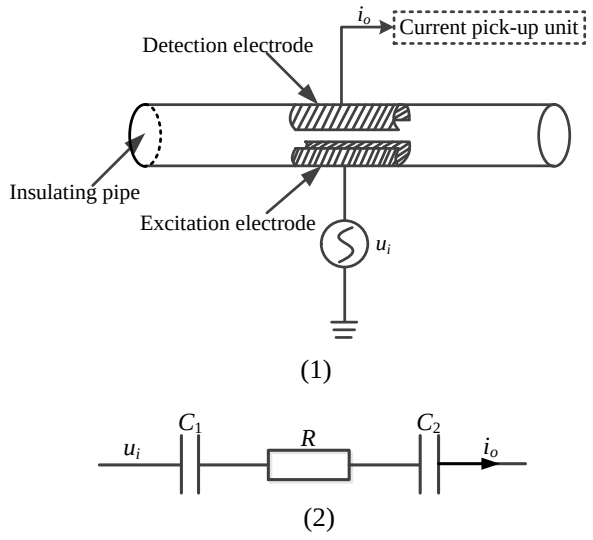

Figure 1. Measurement principle of C^4D technique. (1) Construction of a radial C^4D sensor. (2) The equivalent circuit of the measurement electrode pair.

Currently, a new multi-electrode (12-electrode) contactless resistivity array sensor has been developed based on the C^4D technique [22-24] to measure the resistance of conductive gas-liquid two-phase flow. The electrodes of the sensor are not in contact with the measured fluids, which can overcome the drawbacks of conventional electrical resistance measurement sensors (electrochemical erosion and polarization effect of the electrodes) [25-31]. The 12-electrode

contactless resistivity array sensor is mainly used for tomography at the current stage [22-24, 32]. The research work concerning the void fraction measurement of gas-liquid two-phase flow with this array sensor is limited. Further research is needed.

The aim of this work is to investigate the void fraction measurement of gas-liquid two-phase flow with the 12-electrode contactless resistivity array sensor under five different excitation patterns and seek an effective way to implement void fraction measurement. Experiments of three two-phase distributions will be carried out. The conventional data average method and the principal component regression (PCR) method will be used to establish the void fraction measurement model and implement the void fraction measurement.

2. 12-electrode contactless resistivity array sensor

To investigate the void fraction measurement performance of gas-liquid two-phase flow under five different excitation patterns, a 12-electrode contactless resistivity array sensor is developed. The sensor includes the resistance detection unit, the signal processing unit and a computer, which is shown in Figure 2.

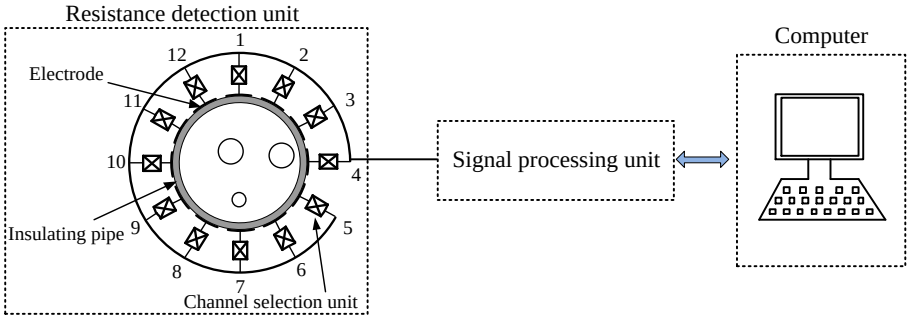

Figure 2. Construction of the 12-electrode contactless resistivity array sensor.

2.1 Five different excitation patterns

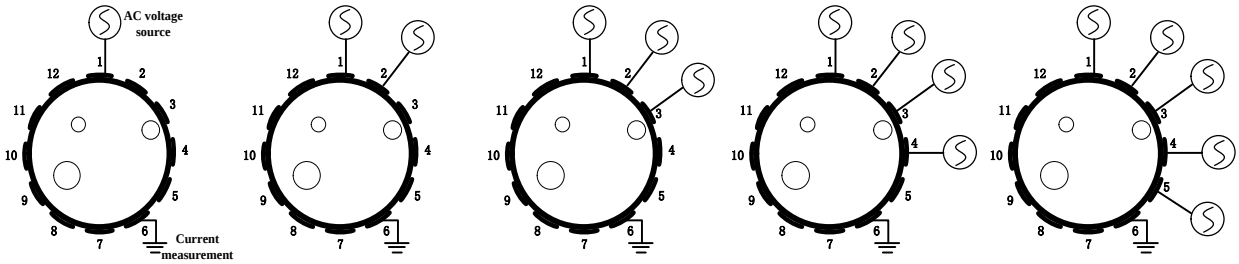

Figure 3. Five excitation patterns. (1) 1-electrode excitation pattern. (2) 2-electrode excitation pattern. (3) 3-electrode excitation pattern. (4) 4-electrode excitation pattern. (5) 5-electrode excitation pattern.

Figure 3 shows the five different excitation patterns which will be investigated in this work, the conventional 1-electrode excitation pattern, the 2-electrode excitation pattern, the 3-electrode excitation pattern, the 4-electrode excitation pattern and the 5-electrode excitation pattern.

Figure 3(1) shows the conventional 1-electrode excitation pattern, the AC voltage source is applied to one electrode and one of the other electrodes is selected as the detection electrode, which forms a measurement electrode pair. Under this excitation pattern, the independent measurement electrode pairs are 1-2 (1 is the excitation electrode, 2 is the detection electrode), 1-3,…, 1-12, 2-3, 2-4,…, 2-12,…, 11-12. An independent measurement is the measurement result corresponding to the independent measurement electrode pair. The number of independent measurement electrode pairs is N=H(H-1)/2, where, H is the number of electrodes. In this work, H=12, N=66.

Figure 3(2) shows the 2-electrode excitation pattern. Under this excitation pattern, all the measurement electrode pairs are: 1&2-3 (1 and 2 are the excitation electrodes, 3 is the detection electrode), 1&2-4, …,1&2-12, 2&3-4, 2&3-5, …, 2&3-1, …, 12&1-2, 12&1-3, …, 12&1-11. For the 2-electrode excitation pattern, N=H(H-2)=120. Similar to the 2-electrode excitation pattern, the numbers of the independent measurement electrode pairs are N=H(H-3)=108, N=H(H-4)=96, N=H(H-5)=84 under the 3-electrode excitation pattern, the 4-electrode

excitation pattern, the 5-electrode excitation pattern, respectively.

2.2 Hardware block of the 12-electrode contactless resistivity array sensor

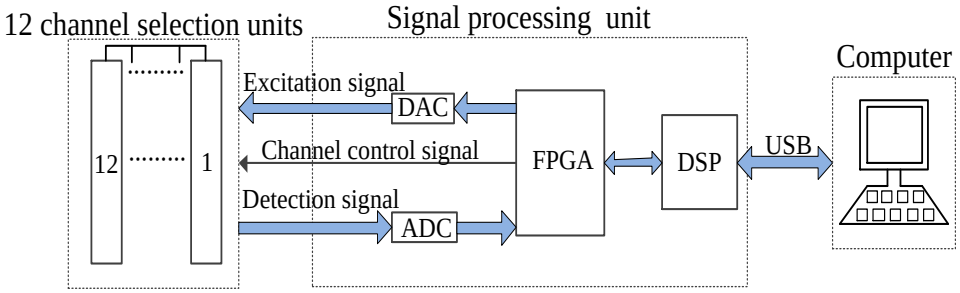

Figure 4. The hardware block of the 12-electrode contactless resistivity array sensor.

Figure 4 shows the hardware block of the 12-electrode contactless resistivity array sensor which includes the channel selection unit, the signal processing unit and a computer, most parts of which are similar to those of the sensors in our previous research works [22, 24]. The main difference is the channel selection unit, with the function of transmitting the excitation signal from the signal processing unit to the excitation electrode, and then sending the detection signal on the detection electrode to the signal processing unit.

The command decoding unit in the channel selection unit is redesigned, the processer of which is Complex Programmable Logic Device (CPLD) (xc9572xl-10vq44). In this work, for each excitation pattern, the sequence number n (n=1, 2,…, N) of each measurement electrode pair matches the state of each electrode (with sequence number h (h=1, 2, …, 12)). When n and h are determined, the state of the hth electrode can be determined (excitation state, detection state or floating state). n can be calculated by the signals from the DSP. Each electrode is connected with a channel selection unit, so h can be calculated in the corresponding channel selection unit. Combining n and h, the CPLD can control the state of each electrode by electronic switches.

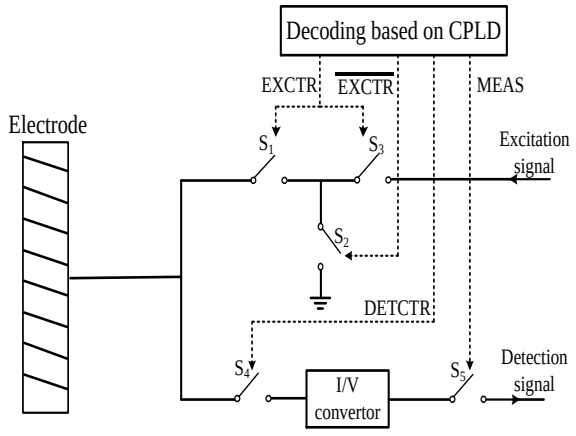

Figure 5. Channel selection unit.

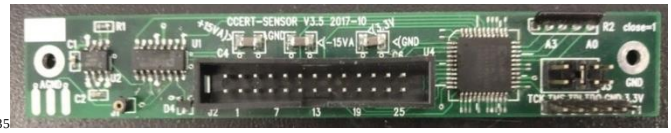

Figure 6. A photo of the channel selection unit.

Figure 5 shows the construction of the channel selection unit. Figure 6 is a photo of the channel selection unit. As shown in Figure 5, the CPLD outputs 4 signals, i.e., the "EXCTR" signal which controls Switch S_1 and Switch S_3, the "$\overline{\text{EXCTR}}$" signal which is the inversion of the "EXCTR" signal and controls Switch S_2, the "DETCTR" signal which controls Switch S_4 and the "MEAS" signal which controls Switch S_5. Each electrode has three states: the excitation state, the detection state and the floating state. When the electrode works as the excitation electrode, Switches S_1 and S_3 are switched on and other switches are switched off. When the electrode works as the detection electrode, Switches S_2, S_4 and S_5 are switched on and other switches are switched off. When the electrode works as the floating state, only Switch S_2 is switched on and other switches are switched off. The function of Switch S_2 is to overcome the influence of the current leakage from Switch S_3 on the measurement result, when the electrode is selected as the detection electrode or floating electrode.

2.3 Detection of the resistance of a measurement electrode pair

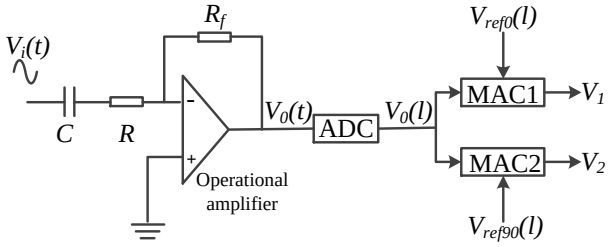

Figure 7. The simplified measurement circuit of the *RC* network.

Figure 7 shows the simplified measurement circuit of *RC* (the equivalent capacitance $C = \frac{C_1 C_2}{C_1 + C_2}$ and resistance R of each measurement) network which is based on the Digital Phase-sensitive Demodulation (DPSD) technique [24]. The calculation process of R is shown as follows:

$$V_i(t) = A_i sin\omega t \tag{1}$$

where, $V_i(t)$ is the excitation voltage, A_i and $\omega = 2\pi f$ are the amplitude and angular frequency of the voltage, respectively. The output voltage of the operational amplifier is:

$$\begin{aligned} V_0(t) &= -\left(\frac{\omega^2 R_f R C^2}{1+\omega^2 R^2 C^2} + j\frac{\omega R_f C}{1+\omega^2 R^2 C^2}\right) V_i(t) \\ &= A_0 \sin(\omega t + \theta) \end{aligned} \tag{2}$$

where, R_f is the feedback resistance, $A_0 = -\frac{\omega R_f A_i C}{\sqrt{\omega^2 R^2 C^2 + 1}}$ and $\theta = arctan\frac{1}{\omega RC}$ are the amplitude and phase of the output signal, respectively

After uniform sampling in the analog-to-digital convertor (ADC), $V_0(t)$ is converted into a discrete voltage signal $V_0(l)$,

$$\boldsymbol{V_0(l) = A_0 sin(\frac{2\pi l}{L} + \theta)} \tag{3}$$

where, l = 0, 1, 2, 3…, L-1, L is the number of samples in a period. Then, $\boldsymbol{V_0(l)}$ is transmitted to the DPSD unit and demodulated with two reference signals $\boldsymbol{V_{ref0}(l)}$ and $\boldsymbol{V_{ref90}(l)}$ in two multiple accumulators (MACs).

$$V_{ref0}(l) = B_1 \sin(\frac{2\pi l}{L}) \tag{4}$$

$$V_{ref90}(l) = B_2 \cos(\frac{2\pi l}{L}) \tag{5}$$

where, $\boldsymbol{B_1}$ and $\boldsymbol{B_2}$ are the amplitudes of the two voltage signals. The $\boldsymbol{V_{ref0}(l)}$ is the corresponding discrete signal of $\boldsymbol{V_i(t)}$. $\boldsymbol{V_{ref90}(l)}$ has a π/2 phase shift relative to $\boldsymbol{V_{ref0}(l)}$. The demodulation process can be described as:

$$\boldsymbol{V_1 = \sum_{l=0}^{L-1} V_0(l) V_{ref0}(l) = \frac{1}{2} L A_0 B_1 cos\theta} \tag{6}$$

$$\boldsymbol{V_2 = \sum_{l=0}^{L-1} V_0(l) V_{ref90}(l) = \frac{1}{2} L A_0 B_2 sin\theta} \tag{7}$$

With Equations (2), (6) and (7), the resistance can be calculated:

$$\boldsymbol{R = -\frac{L V_1 R_f A_i}{2 B_1 [\left(\frac{V_1}{B_1}\right)^2 + \left(\frac{V_2}{B_2}\right)^2]}} \tag{8}$$

2.4 Measurement duration under different excitation patterns

In this work, the numbers of measurements under different excitation patterns are different, so the time of the measurement process under different excitation patterns is different. Here, the time of sampling and transmitting of the N measurements under each excitation pattern is

$$\boldsymbol{T_0 = N T_1 + T_2} \tag{9}$$

Where, $\boldsymbol{T_1}$ is the time of the channel selection (turning on/off the switches), signal sampling and storage, data calculation and transmitting, i.e., the process to obtain one measurement. It can be calculated by the following equation:

$$\boldsymbol{T_1 = T_{11} + T_{12} + T_{13}} \tag{10}$$

Where, $\boldsymbol{T_{11}}$ is the transition time of channel selection, $\boldsymbol{T_{11} \approx 9.63\mu s}$. $\boldsymbol{T_{12}}$ is the time of signal sampling by ADC and signal storage to FPGA, $\boldsymbol{T_{12} \approx 19.55\mu s}$. $\boldsymbol{T_{13}}$ is the time of DPSD and the time for DSP to read the data calculated by DPSD in FPGA, $\boldsymbol{T_{13} \approx 2.70\mu s}$. So $\boldsymbol{T_1 \approx 31.88\mu s}$. $\boldsymbol{T_2}$ is the time of packing one frame data (consisting of N measurements) and sending them from DSP to computer through USB, $\boldsymbol{T_2 \approx 39.40\mu s}$. The values of $\boldsymbol{T_{11}}$, $\boldsymbol{T_{12}}$, $\boldsymbol{T_{13}}$ and $\boldsymbol{T_2}$ are obtained by experiments. $\boldsymbol{T_0}$ under each excitation pattern is listed in Table 1.

Table 1. T_0 under each excitation pattern

Excitation pattern	N	$\boldsymbol{T_0(\mu s)}$
1-electrode excitation pattern	66	2143.48
2-electrode excitation pattern	120	3865.00
3-electrode excitation pattern	108	3482.44
4-electrode excitation pattern	96	3099.88
5-electrode excitation pattern	84	2717.32

As shown in Table 1, the measurement processes of the 1-electrode excitation pattern and the 2-electrode excitation pattern are respectively the least and the most time-consuming. And, the 5-electrode excitation pattern has the least measurement duration among the multi-electrode excitation patterns.

3. Void fraction measurement method

In the research field of two-phase flow, using multi-electrode array sensors for void fraction measurement of gas-liquid two-phase flow has a long history and there are many data processing methods [1-19]. Among these methods, the data average method [3-6, 8, 9, 14, 19] and the principal component regression (PCR) method [12, 33-41] are the two most commonly used. So in this work, the data average

method and the PCR method are adopted to establish the void fraction measurement model. To overcome the influence of phase distributions on the measurement of void fraction, a specified void faction measurement model will be established for each phase distribution under each excitation pattern.

3.1 Pre-processing of data

After obtaining the experimental resistance data by the 12-electrode contactless resistivity array sensor, the resistance data are pre-processed by Equation (11):

$$p_n = \frac{R_n - R_{0n}}{R_{0n}},\ n=1, 2, \ldots, N. \tag{11}$$

Where, R_{0n} is the value of the measurement resistance when the pipe is filled with tap water, R_n is the measurement resistance when the distribution in the pipe is unknown, N is the number of measurements under each excitation pattern.

3.2 The data average method

To establish the void fraction measurement model by the data average method under each excitation pattern [3-6, 8, 9, 14, 19], the mean value of all the p_n is calculated:

$$\bar{p} = \frac{\sum_{n=1}^{N} p_n}{N} \tag{12}$$

Then the void fraction measurement model can be established by the calibration curve between the void fraction α and the $\bar{p}$. Thus the void fraction measurement can be implemented according to the established model.

The void fraction measurement models of different phase distributions under different excitation patterns are established respectively.

3.3 The principal component regression (PCR) method

The principal component regression (PCR) method is a modeling method which has been widely used in the research field of parameter measurement of multiphase flow [12, 33-41].

With the PCR method, the void fraction measurement model can be described as:

$$\alpha = \beta_1 s_1 + \beta_2 s_2 + \cdots + \beta_M s_M + t \tag{13}$$

where, α is the value of void fraction, $s_1, s_2, \ldots, s_M$ are the principal components, $\beta_1, \beta_2, \ldots, \beta_M$ are the weight coefficients of the M principal components and t is the bias coefficient.

The number M, the weight coefficients and the bias coefficient are pre-determined by a learning process with learning samples.

Let $\boldsymbol{P} = \begin{bmatrix} p_{11}\ p_{12} \ldots p_{1N} \\ p_{21}\ p_{22} \ldots p_{2N} \\ \vdots\ \ \vdots\ \ \ \vdots \\ p_{K1}\ p_{K2} \ldots p_{KN} \end{bmatrix}$ be the learning sample matrix. Where, each row of the matrix is a sample, K is the number of samples, N is the number of variables of each sample. Principal component analysis (PCA) method is used to determine the principal components $s_1, s_2, \ldots, s_M$ and the number M [12, 33-38]. The purpose of PCA is to find principal components which can reveal the most information of original data and each principal component is the linear combination of the original variables [12, 33-38]. In this work, the dimension of original variables is N. Let $\boldsymbol{Q} = \mathrm{cov}(\boldsymbol{P})$ be the covariance matrix of $\boldsymbol{P}$. $\boldsymbol{Q}$ has N characteristic roots $\lambda_1 > \lambda_2 > \cdots > \lambda_N$ corresponding to N orthonormal unit characteristic vectors $\boldsymbol{u}_1, \boldsymbol{u}_2, \ldots, \boldsymbol{u}_N$, $\boldsymbol{u}_i = [u_{1i}, u_{2i}, \ldots, u_{Ni}]^{\mathrm{T}}, i = 1, 2, \ldots, N$. To determine the number of principal components M, the rule is that the overall variance contribution rate of the first M principal components is larger than γ (in this work, γ=97.5%) [12, 33-38]. The matrix of the first M orthonormal unit characteristic vectors is $\boldsymbol{U} = \begin{bmatrix} u_{11}\ u_{12} \ldots u_{1M} \\ u_{21}\ u_{22} \ldots u_{2M} \\ \vdots\ \ \vdots\ \ \ \vdots \\ u_{N1}\ u_{N2} \ldots u_{NM} \end{bmatrix}$. Then, for the kth sample $\boldsymbol{p}_k = [p_{k1}, p_{k2}, \ldots, p_{kN}]$, $k = 1, 2, \ldots, K$, the corresponding M principal components can be calculated according to the following equation:

$$s_{kj} = \sum_{i=1}^{N} p_{ki} u_{ij} \tag{14}$$

where, s_{kj} is the jth principal component of the kth sample, $j = 1, 2, \ldots, M$.

After the values of principal components and number M are obtained, the weight coefficients and the bias coefficient can be determined by solving the following optimization problem:

$$J = \|\boldsymbol{G}\boldsymbol{\delta} - \boldsymbol{\alpha}\|^2 \rightarrow min \tag{15}$$

where, $\boldsymbol{G} = \begin{bmatrix} s_{11}\ s_{12} \ldots s_{1M}\ 1 \\ s_{21}\ s_{22} \ldots s_{2M}\ 1 \\ \vdots\ \ \vdots\ \ \ \vdots\ \ \vdots \\ s_{K1}\ s_{K2} \ldots s_{KM}\ 1 \end{bmatrix}$, $\boldsymbol{\delta} = [\beta_1, \beta_2, \ldots, \beta_M, t]^{\mathrm{T}}$, $\boldsymbol{\alpha} = [\alpha_1, \alpha_2, \ldots, \alpha_K]^{\mathrm{T}}$ is the void fraction vector of the learning samples. $\boldsymbol{\delta} = [\beta_1, \beta_2, \ldots, \beta_M, t]^{\mathrm{T}}$ can be determined by the least square method [40-41]:

$$\boldsymbol{\delta} = (\boldsymbol{G}^{\mathrm{T}}\boldsymbol{G})^{-1}\boldsymbol{G}^{\mathrm{T}}\boldsymbol{\alpha} \tag{16}$$

Thus, all the coefficients of Equation (13) are obtained by the learning process..

In practical void fraction measurement, N measurements are obtained and pre-processed according to Equation (11). Then the principal components are calculated according to the pre-determined matrix $\boldsymbol{U}$ and Equation (14). Thus the

estimated value of void fraction can be calculated according to the pre-determined coefficients and the corresponding void fraction measurement model (i.e. Equation (13)).

According to Equations (13)~(16), different void fraction measurement models are established for different phase distributions under different excitation patterns, respectively.

3.4 Evaluation Index

To evaluate the performance of void fraction measurement, the absolute error E of void fraction measurement is introduced in this work [10, 14]. It can be defined as:

$$E = \hat{\alpha} - \alpha \tag{17}$$

Where, α is the reference value of void fraction, $\hat{\alpha}$ is the estimated value of void fraction.

4. Experiments

4.1 Experimental setup

The 12-electrode contactless resistivity array sensor mentioned above is used to implement the experiments. The 12-electrode contactless resistivity detection unit consists of an insulating pipe and an electrode array which includes 12 electrodes. Each electrode is made of a rectangular copper foil with the length of 125 mm and the electrode angle is 25°. Each electrode is connected with a channel selection unit. The insulating pipe is a PVC pipe and its outer diameter and wall thickness are 110 mm and 2 mm respectively. The frequency of excitation voltage is $f = 500$kHz in this work.

Three typical cross-sectional phase distributions are investigated in this work, i.e., the bubble flow, the stratified flow and the annular flow, as is shown in Figure 8.

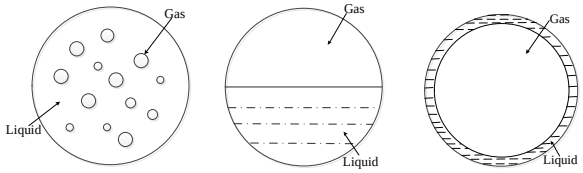

(1) (2) (3)

Figure 8. Three cross-sectional phase distributions. (1). bubble flow; (2). stratified flow; (3). annular flow.

Tap water and some plastic rods with different diameters are used to simulate the three different two-phase distributions mentioned above. The 12-electrode contactless resistivity array sensor is used to obtain the measurement resistances.

1) Put some small rods into the optional area of the water in the pipe vertically to simulate the bubble flow. The reference values of void fraction are obtained by the ratio of area sum of rods to the area of the inner cross section of the pipe.

2) Place the pipe horizontally and adjust the volume of the water in the pipe to simulate the stratified flow. The reference values of void fraction are obtained by the ratio of the volume of air in the sensor to the volume of the pipe.

3) Put one large plastic rod into the water to simulate the annular flow and the reference value of void fraction is obtained by the ratio of the area of the cross section of the rod to the area of the inner cross section of the pipe.

4.2 Experimental results

4.2.1 Experimental results by data average method

Figure 9 shows the void fraction measurement results by data average method of the three two-phase distributions under the five different excitation patterns. For each figure, the abscissa shows the reference value of void fraction, the ordinate shows the estimated value of void fraction. Table 2 shows the absolute error ranges of void fraction measurement by data average method of the three two-phase distributions under the five different excitation patterns.

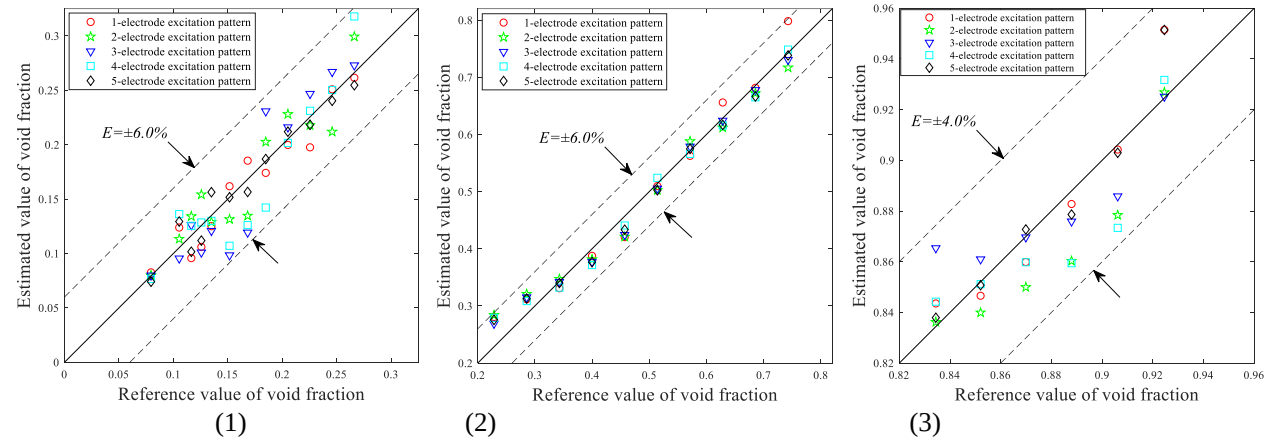

(1) (2) (3)

Figure 9. Void fraction measurement results by data average method of the three two-phase distributions under the five different excitation patterns. (1). Bubble flow; (2). Stratified flow; (3). Annular flow.

Table 2. Absolute error ranges of void fraction measurement of the three two-phase distributions by data average method under the five different excitation patterns

Excitation patterns	Absolute error range of bubble flow	Absolute error range of stratified flow	Absolute error range of annular flow
1-electrode excitation pattern	[-2.80, 1.85]%	[-3.67, 5.55]%	[-1.00, 2.70]%
2-electrode excitation pattern	[-3.40, 3.31]%	[-3.60, 5.53]%	[-2.78, 0.23]%
3-electrode excitation pattern	[-5.32, 4.59]%	[-3.28, 4.05]%	[-2.03, 3.10]%
4-electrode excitation pattern	[-4.45, 5.17]%	[-2.84, 5.06]%	[-3.28, 0.98]%
5-electrode excitation pattern	[-1.49, 2.40]%	[-2.37, 4.72]%	[-0.93, 2.69]%

According to the void fraction measurement results by data average method, it can be found that for bubble flow, the absolute values of errors under the 1-electrode excitation pattern and the 5-electrode excitation pattern are all less than 3.0%. Meanwhile, the void fraction measurement performance of the bubble flow under the 2-electrode excitation pattern is better than those under the 3-electrode excitation pattern and the 4-electrode excitation pattern. For stratified flow, the absolute values of errors under the 3-electrode excitation pattern and the 5-electrode excitation pattern are all less than 5.0%. For annular flow, the absolute values of errors under the 1-electrode excitation pattern, the 2-electrode excitation pattern and the 5-electrode excitation pattern are all less than 3.0%. To conclude, the 5-electrode excitation pattern is the best choice and all the absolute values of void fraction measurement errors are less than 5.0%.

4.2.2 Experimental results by PCR method

Figure 10 shows the void fraction measurement results by PCR method of the three two-phase distributions under the five different excitation patterns. For each figure, the abscissa shows the reference value of void fraction, the ordinate shows the estimated value of void fraction. Table 3 shows the absolute error ranges of void fraction measurement by PCR method of the three two-phase distributions under the five different excitation patterns.

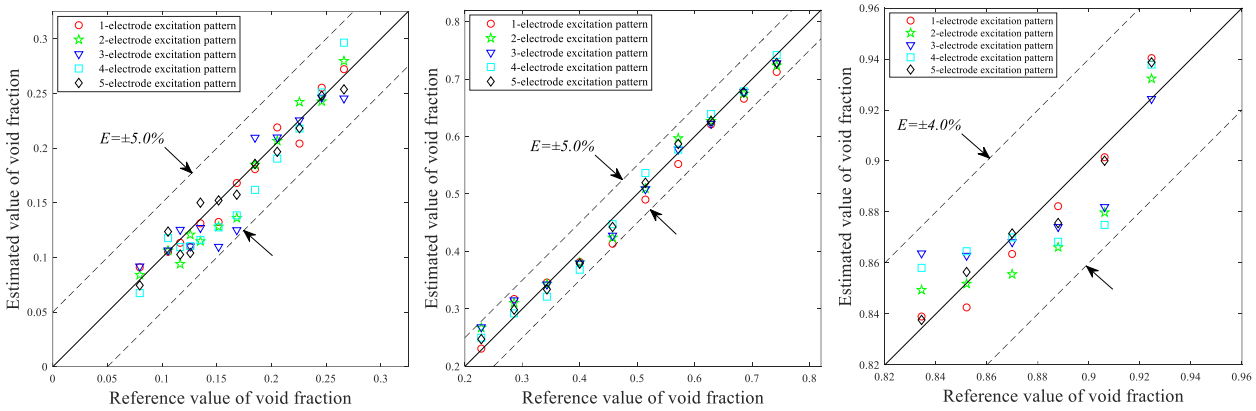

Figure 10. Void fraction measurement results by PCR method of the three two-phase distributions under the five different excitation patterns. (1). Bubble flow; (2). Stratified flow; (3). Annular flow.

Table 3. Absolute error ranges of void fraction measurement of the three two-phase distributions by PCR method under the five different excitation patterns

Excitation patterns	Absolute error range of bubble flow	Absolute error range of stratified flow	Absolute error range of annular flow
1-electrode excitation pattern	[-2.14, 1.37]%	[-4.37, 3.16]%	[-0.95, 1.58]%
2-electrode excitation pattern	[-3.22, 1.67]%	[-3.31, 3.86]%	[-2.63, 1.50]%
3-electrode excitation pattern	[-4.33, 2.47]%	[-2.94, 3.97]%	[-2.42, 2.94]%
4-electrode excitation pattern	[-2.98, 3.02]%	[-3.17, 2.22]%	[-3.12, 2.37]%
5-electrode excitation pattern	[-2.17, 1.82]%	[-2.12, 1.88]%	[-1.23, 1.41]%

According to the void fraction measurement results by PCR method, for bubble flow, the absolute values of errors under the 1-electrode excitation pattern and the 5-electrode excitation pattern are all less than 3.0%. For stratified flow, the absolute values of errors under the 5-electrode excitation pattern are all less than 3.0%. For annular flow, the absolute values of errors under the 1-electrode excitation pattern and the 5-electrode excitation pattern are all less than 2.0%. To conclude, the 5-electrode excitation pattern is still the best choice and all the absolute values of void fraction measurement errors are less than 3.0%.

4.3 Discussions

The above experimental results show that the 12-electrode contactless resistivity array sensor is feasible and effective for the void fraction measurement of gas-liquid two-phase flow.

According to the research results, useful information can be obtained, covering several aspects.

The research results indicate that different excitation patterns have different void fraction measurement performances. Among the five excitation patterns, the 5-electrode excitation pattern has the best overall void fraction measurement performance no matter which of the two data processing methods is used. The absolute values of void fraction measurement errors under the 5-electrode excitation pattern are less than 5.0% and 3.0% by the data average method and the PCR method, respectively. The measurement duration under the 5-electrode excitation pattern is also satisfactory as can be found in Table 1. Besides, it is necessary to point out that the experimental results also indicate an interesting fact. The 1-electrode excitation pattern, which is the most widely used excitation pattern in the research field of gas-liquid two-phase flow, shows no obvious advantages, especially for the stratified flow. The absolute values of void fraction measurement errors under the 1-electrode excitation pattern are less than 6.0% and 5.0% by the data average method and the PCR method, respectively. To the best of the authors' experience and knowledge, there are two possible reasons. One is that the measurement performance of 1-electrode excitation pattern is easily affected by phase distributions, especially much more sensitive to the stratified flow. The other is that the intensity of measurement signal under the 1-electrode excitation pattern is much lower than that under the 5-electrode excitation pattern.

Meanwhile, for all the excitation patterns investigated in this work, it can be found that the two used data processing methods (the data average method and the PCR method) are both effective. Using data average method, the absolute values of void fraction measurement errors are less than 6.0%. Using PCR method, the absolute values of void fraction measurement errors are less than 5.0%. Relatively speaking, the overall void fraction measurement performance by the PCR method is better than that by the data average method, as listed in Table 2 and 3. That may benefit from the more effective and sufficient information utilization of the PCR method.

Besides, the research results indicate that the combination of the 5-electrode excitation pattern and the PCR method has the best overall void fraction measurement performance with satisfactory measurement duration. According to the experimental results, the absolute values of void fraction measurement errors of the bubble flow, the stratified flow and the annular flow by using this combination are less than 3.0%, 3.0% and 2.0%, respectively. This is mainly attributed to better information utilization efficiency and higher excitation signal intensity.

It is necessary to mention that the research results also indicate a unexpected/strange phenomenon, i.e., the 2-electrode excitation pattern, the 3-electrode excitation pattern and the 4-electrode excitation pattern don't have better overall void fraction measurement performance than the 1-electrode excitation pattern. At the current stage, the research results don't show a certain rule to follow. Meanwhile, based on the authors' experience and knowledge, we couldn't provide a reasonable interpretation/description. It is a complex problem which may concern about the excitation signal intensity, the sensitivities under different excitation patterns, and the soft-field characteristics (This specific term is usually used in the research field of electrical tomography. The sensitivity

distributions of electrical tomography systems are affected by the phase distributions. Especially in stratified flow, the sensitivity distributions would be distorted more seriously). Further research is needed in future to reveal the answer.

5. Conclusions:

The void fraction measurement of gas-liquid two-phase flow by a 12-electrode contactless resistivity array sensor is investigated in this work. A 12-electrode contactless resistivity array sensor is developed to implement five different excitation patterns (the 1-electrode excitation pattern, the 2-electrode excitation pattern, the 3-electrode excitation pattern, the 4-electrode excitation pattern and the 5-electrode excitation pattern). Three two-phase distributions (the bubble flow, the stratified flow and the annular flow) are investigated. The data average method and the PCR method are adopted to establish the void fraction measurement models and implement void fraction measurement. Experiments with different void fractions are carried out. The research results indicate that using the 12-electrode contactless resistivity array sensor to measure void fraction of gas-liquid two-phase flow is an effective approach. According to the research results, the following conclusions are obtained:

1). The void fraction measurement performances of the 12-electrode contactless resistivity array sensor under different excitation patterns are different. Among the five excitation patterns, the 5-electrode excitation pattern has the best overall void fraction measurement performance no matter which data processing method is used.

2). Comparing the void fraction measurement results obtained by using the two data processing methods, the overall void fraction measurement performance by the PCR method is better than that by the data average method.

3). Among all the combinations of the excitation pattern and the data processing method, the 5-electrode excitation pattern+PCR combination has the best overall void fraction measurement performance. With this combination, the absolute values of void fraction measurement errors of the bubble flow, the stratified flow and the annular flow are less than 3.0%, 3.0% and 2.0%, respectively.

This work provides an effective approach for void fraction measurement of gas-liquid two-phase flow. Compared with conventional void fraction measurement methods based on contact conductivity measurement, the 12-electrode contactless resistivity array sensor in this work can implement the void fraction measurement contactlessly and avoid the negative effects of electrochemical erosion and polarization of the electrodes.

Useful knowledge and experience have been obtained, which can provide reference for other research works. To further improve the void fraction measurement performance of the 12-electrode contactless resistivity array sensor, electrical tomography technique and new data processing methods (e.g. time sequence learning method and Bayesian learning method [42, 43]) should be introduced and investigated. That would be our further research work in future.

Acknowledgements

This work was supported by the National Nature Science Foundation of China (No. 51976189).

References

[1] Crowe C T 2006 Multiphase flow handbook *CRC Press*.
[2] Powell RL 2008 Experimental techniques for multiphase flows *Phys Fluids* **20** 040605.
[3] Ceccio S L George D L 1996 A Review of Electrical Impedance Techniques for the Measurement of Multiphase Flows *Journal of Fluids Engineering* **118** 391-399.
[4] Thorn R Johansen G A Hammer E A 1997 Recent developments in three-phase flow measurement. *Measurement Science and Technology* **8** 691-701.
[5] Merilo M Dechene RL Cichowlas WM 1977 Void Fraction Measurement With a Rotating Electric Field Conductance Gauge *Journal of Heat Transfer-Transactions Of The ASME* **99** 330-332.
[6] Tournaire A 1986 Dependence of the instantaneous response of impedance probes on the local distribution of the void fraction in a pipe *International Journal of Multiphase Flow* **12** 1019-1024.
[7] Andreussi P Bendiksen K 1989 An investigation of void fraction in liquid slugs for horizontal and inclined gas—liquid pipe flow *International Journal of Multiphase Flow* **15** 937-946.
[8] Saiz-Jabardo J M Bouré J A 1989 Experiments on void fraction waves *International Journal of Multiphase Flow* **15** 483-493.
[9] Chase G G Willis M S Kannel J 1990 Averaging volume size determination of electroconductive porosity probes *International Journal of Multiphase Flow* **16** 103-112.
[10] Fossa M 1998 Design and performance of a conductance probe for measuring the liquid fraction in two-phase gas-liquid flows *Flow Measurement and Instrumentation* **9** 103-109.
[11] Devia F Fossa M 2003 Design and optimisation of impedance probes for void fraction measurements. *Flow Measurement and Instrumentation* **14** 139-149.
[12] Dong F Jiang Z X Qiao X T et al. 2003 Application of Electrical Resistance Tomography to Two-phase Pipe Flow Parameters Measurement *Flow Measurement and Instrumentation* **14** 183-192.
[13] Cho J Perlin M Ceccio S L 2005 Measurement of near-wall stratified bubbly flows using electrical impedance *Measurement Science and Technology* **16** 1021.
[14] Rocha M S et al. 2010 Void Fraction Measurement and Signal Analysis from Multiple-Electrode Impedance Sensors *Heat Transfer Engineering* **29** 924-935.
[15] Borges J E Pereira N H C Matos J 2010 Performance of a combined three-hole conductivity probe for void fraction and velocity measurement in air–water flows *Experiments in fluids* **48** 17-31.
[16] Zhao T Iso Y Ikeda R 2019 Real-time measurement of particle volume fraction in centrifugal fields by wireless electrical

resistance detector *Flow Measurement and Instrumentation* **65** 90-97.
[17] Dang Z Zhao Y Wang G et al. 2019 Investigation of the effect of the electrode distance on the impedance void meter performance in the two-phase flow measurement *Experimental Thermal and Fluid Science* **101** 283-295.
[18] Dang C Darnajou M Bellis C et al. 2019 Numerical and experimental analysis of the correlation between EIT data eigenvalues and two-phase flow phase fraction *Measurement Science and Technology* **31** 015302.
[19] Forte G Alberini Federico Simmons Mark J H 2019 Measuring gas hold-up in gas-liquid/gas-solid-liquid stirred tanks with an electrical resistance tomography linear probe *Aiche Journal* **65**.
[20] Kubáň P Hauser P C 2018 20th anniversary of axial capacitively coupled contactless conductivity detection in capillary electrophoresis *TrAC Trends in Analytical Chemistry* **102** 311-321.
[21] Kubáň P Hauser P C 2019 Contactless conductivity detection for analytical techniques: Developments from 2016 to 2018 *Electrophoresis* **40** 124-139.
[22] Wang B L Hu Y Y Ji H F Huang Z Y Li H Q 2013 A novel electrical resistance tomography system based on C4D technique *IEEE Trans Instrum Meas* **62** 1017-1024.
[23] Wahab Abdul Y et al 2018 Optimisation of electrode dimensions of ERT for non-invasive measurement applied for static liquid–gas regime identification *Sens. Actuators A* **270** 50-64.
[24] Wang Y X Wang B L Huang Z Y Ji H F Li H Q 2018 New capacitively coupled electrical resistance tomography (CCERT) system *Measurement Science and Technology* **29** 104007.
[25] Holder D S 2005 Electrical impedance tomography *IOP*.
[26] Wahab Y A Rahim R A Rahiman M H F et al 2015 Non-invasive process tomography in chemical mixtures – A review *Sensors & Actuators B Chemical* **210** 602-617.
[27] Aw S R Rahim R A Rahiman M H F et al 2014 Electrical resistance tomography: A review of the application of conducting vessel walls[J] *Powder Technology* **254** 256-264.
[28] Wang M Wang Q and Karki B 2016 Arts of electrical impedance tomographic sensing *Philos Trans Roy Soc London A Math Phys Sci* **374** 20150329.
[29] Wang R C Frias M A R Wang H G Yang W D Ye J M 2018 Evaluation of electrical resistance tomography with voltage excitation compared with electrical capacitance tomography *Meas Sci Technol* **29** 125401.
[30] Wei K H Qiu C H Primrose K 2016 Super-sensing technology: Industrial applications and future challenges of electrical tomography *Philos Trans Roy Soc A Math Phys Eng Sci* **374** 602-617.
[31] Soleimani M 2016 Super-sensing through industrial process tomography *Philos Trans A Math Phys Eng Sci* **374** 20150445.
[32] Xu Z Jiang Y D Wang B L et al. 2018 Image Reconstruction Performance of a 12-Electrode CCERT Sensor Under Five Different Excitation Patterns *IEEE Access* **6** 65783-65795.
[33] Lattin J M Carroll D J Green P E 2003 Analyzing multivariate data *Cengage Learning, Inc.*
[34] Johnson D E 1998 Applied multivariate methods for data analysis *Duxbury Press.*
[35] Mosdorf R Górski G 2016 Identification of two-phase flow patterns in minichannel based on RQA and PCA analysis. *International Journal of Heat and Mass Transfer* **96** 64-74.
[36] Zbilut J P Giuliani A Webber J C L 1997 Recurrence Quantification Analysis and Principal Components in the Detection of Short Complex Signals *Physics Letters A* **237**.
[37] Cao L J Chua K S Chong W K et al. 2003 A comparison of PCA, KPCA and ICA for dimensionality reduction in support vector machine *Neurocomputing* **55** 321-336.
[38] Blum M G B Nunes M A Prangle D Sisson S A 2013 A Comparative Review of Dimension Reduction Methods in Approximate Bayesian Computation *Statistical Science* **28** 189-208.
[39] Morris J S 2015 Functional Regression *Annu Rev Stat Appl* **2** 321–359.
[40] Fletcher R 1987 Practical methods of optimization *Wiley*.
[41] Kutner M H Nachtsheim C J Neter J 2004 Applied linear regression models *McGraw-Hill Education.*
[42] Gagnon H Grychtol B Adler A 2015 A comparison framework for temporal image reconstructions in electrical impedance tomography *Physiological Measurement* **36** 1093.
[43] Liu S Jia J Zhang Y D et al. 2018 Image reconstruction in electrical impedance tomography based on structure-aware sparse Bayesian learning *IEEE Transactions on Medical Imaging* **37** 2090-2102.